STEM CELLS AND DEVELOPMENT
Volume 24, Number 22, 2015

DOI: 10.1089/scd.2015.0104

Peripheral Nerve Regeneration by Secretomes of Stem Cells from Human Exfoliated Deciduous Teeth

Yukiko Sugimura-Wakayama,[1] Wataru Katagiri,[1] Masashi Osugi,[1] Takamasa Kawai,[1] Kenichi Ogata,[1,2] Kohei Sakaguchi,[1] and Hideharu Hibi[1]

Peripheral nerve regeneration across nerve gaps is often suboptimal, with poor functional recovery. Stem cell transplantation-based regenerative therapy is a promising approach for axon regeneration and functional recovery of peripheral nerve injury; however, the mechanisms remain controversial and unclear. Recent studies suggest that transplanted stem cells promote tissue regeneration through a paracrine mechanism. We investigated the effects of conditioned media derived from stem cells from human exfoliated deciduous teeth (SHED-CM) on peripheral nerve regeneration. In vitro, SHED-CM-treated Schwann cells exhibited significantly increased proliferation, migration, and the expression of neuron-, extracellular matrix (ECM)-, and angiogenesis-related genes. SHED-CM stimulated neuritogenesis of dorsal root ganglia and increased cell viability. Similarly, SHED-CM enhanced tube formation in an angiogenesis assay. In vivo, a 10-mm rat sciatic nerve gap model was bridged by silicon conduits containing SHED-CM or serum-free Dulbecco's modified Eagle's medium. Light and electron microscopy confirmed that the number of myelinated axons and axon-to-fiber ratio (G-ratio) were significantly higher in the SHED-CM group at 12 weeks after nerve transection surgery. The sciatic functional index (SFI) and gastrocnemius (target muscle) wet weight ratio demonstrated functional recovery. Increased compound muscle action potentials and increased SFI in the SHED-CM group suggested sciatic nerve reinnervation of the target muscle and improved functional recovery. We also observed reduced muscle atrophy in the SHED-CM group. Thus, SHEDs may secrete various trophic factors that enhance peripheral nerve regeneration through multiple mechanisms. SHED-CM may therefore provide a novel therapy that creates a more desirable extracellular microenvironment for peripheral nerve regeneration.

Introduction

Peripheral nerve injury (PNI) is caused by trauma or surgical complications [1,2]. After PNI, distal stump demyelination and degradation occur, leading to target muscle atrophy and loss of functionality. Natural regeneration may occur over short nerve gaps (1–2 mm). Direct end-to-end nerve suture is performed for nerve gaps of <5 mm [3,4]. Tensionless suturing is required for successful nerve repair. However, a graft is necessary for nerve regeneration across large gaps.

At present, autologous nerve grafts are considered as the gold standard for functional nerve regeneration. However, autologous nerve grafts have several drawbacks, including tissue supply, loss of sensation at the donor site, mismatch between the recipient site and donor nerve, and possible formation of a painful neuroma [5,6]. Therefore, new approaches for PNI treatment are desired.

Both cellular and molecular events occur during the initial process of peripheral nerve regeneration [7]. Macrophages, a phenotypically diverse population of immune cells, are integrated into both nerve degeneration and regeneration [8–10]. Macrophages reach the injury site within 24 h and reach a peak number within 2–3 days [11,12]. In PNI, macrophages, which are mainly recruited from circulation, disrupt and phagocytose axons, produce growth factors, and promote the migration of Schwann cells (SCs) [1,13]. SCs have been identified as the major glial cells in peripheral nerve systems and play a central role in axonal regrowth through various mechanisms. SCs also participate in the phagocytosis of axonal and myelin debris during the first few days after injury [14]. SCs produce various neurotrophic factors (NTFs), cytokines [15], and extracellular matrix (ECM) and adhesion molecules [16] that lead to axonal regeneration. Regenerating axons extend to the target organs, leading to functional reinnervation.

Stem cell transplantation therapy is an effective strategy for tissue regeneration. Various types of transplanted stem cells were shown to enhance peripheral nerve regeneration in

[1]Department of Oral and Maxillofacial Surgery, Nagoya University Graduate School of Medicine, Nagoya, Japan.
[2]Section of Oral and Maxillofacial Oncology, Division of Maxillofacial Diagnostic and Surgical Sciences, Faculty of Dental Science, Kyushu University, Fukuoka, Japan.

preclinical animal studies of nerve reconstruction. A variety of cell types, such as bone marrow stromal cells, adipose-derived stromal cells, muscle-derived stem cells, and dental pulp stem cells, were applied to this approach [17–24]. However, recent studies have reported low transplanted stem cell survival rates. For example, a study of stem cell transplantation in spinal cord injury revealed that the transplanted cells survived for only 1–2 weeks [25]. In a mouse model of demyelinating disease, multiple sclerosis, the transplanted cells could no longer be identified after 8 days [26]. In addition, the transplanted stem cells exhibit poor differentiation [27]. Stem cells secrete various growth factors and cytokines known as secretomes [28–30]. These secretomes can be detected in stem cell-cultured conditioned medium (CM). Therefore, CM containing secretomes could be used in promising regenerative therapies. Previous studies have reported that CM from various stem cells effectively treated hypoxic brain injury [31], focal cerebral ischemia [32], and spinal cord injury [33]. We previously reported that CM promoted bone growth [34,35] and periodontal tissue regeneration [36,37] and improved bisphosphonate-related osteonecrosis of the jaw in a rat model [38].

Stem cells from human exfoliated deciduous teeth (SHEDs) harbor a self-renewal capability [39] and exist within a perivascular niche in the dental pulp. SHEDs have a high capacity for proliferation and can differentiate into a variety of cell types, including neural cells, adipocytes, osteoblasts, and chondrocytes [40,41]. SHEDs secrete trophic factors that promote neuronal migration, induce vasculogenesis [32], promote axon regeneration [40], and protect neurons from apoptosis [33]. Therefore, these previous studies support the use of SHEDs as a potential cellular resource for peripheral nerve regeneration therapies.

The present study focuses on CM containing paracrine factors secreted by cultured SHEDs. Herein, we examined the influences of SHED-CM on dorsal root ganglion (DRG) neurons and SCs in vitro. Moreover, we investigated the ability of SHED-CM to stimulate nerve regeneration in vivo in a rat sciatic nerve defect model.

Materials and Methods

Ethics statement

Exfoliated deciduous teeth were collected under guidelines approved by Nagoya University (H-73, 2003). Ethical approval was obtained from the Ethics Committee of Nagoya University (permission number 8–2).

All experimental procedures involving animals were conducted according to the National Institutes of Health Guide for the Care and Use of Laboratory Animals and were approved by the Nagoya University School of Medicine Animal Care and Use Committee.

Isolation of SHEDs and cell culture

Human SHEDs were isolated as described previously [41]. In brief, human exfoliated deciduous teeth were collected from patients aged 6–12 years. All patients provided written informed consent. The dental pulp was separated from the crown and root. The isolated pulp was subsequently digested in a solution of 3 mg/mL of collagenase type I and 4 mg/mL of dispase for 1 h at 37°C. Single-cell suspensions were cultured in Dulbecco's modified Eagle's medium (DMEM; Gibco, Rockville, MD) supplemented with 10% fetal bovine serum (FBS) and antibiotic–antimycotic solution (100 units/mL penicillin G, 100 μg/mL streptomycin, and 0.25 μg/mL amphotericin B; Gibco) and incubated at 37°C in an atmosphere of 5% CO_2/95% air.

The primary characteristics of the SHEDs were assessed by flow cytometry as described previously [40]. The SHEDs exhibited fibroblastic morphology with a bipolar spindle shape. Flow cytometry revealed that the SHEDs expressed the mesenchymal stem cell markers, CD90, CD73, and CD105, but not the endothelial/hematopoietic markers, CD34, CD45, CD11b/c, and human leukocyte antigen HLA-DR. The SHEDs efficiently differentiated adipogenic, chondrogenic, and osteogenic lineages. Majority of SHEDs coexpressed several neural lineage markers, nestin, doublecortin, β-III-tubulin, NeuN, GFAP, S-100, A2B5, and CNPase, but not adenomatous polyposis or myelin basic protein.

Preparation of CM

After the SHEDs reached 80% confluency, the medium was replaced with serum-free DMEM containing antibiotic–antimycotic solution. This cell-cultured CM was collected after a 48-h incubation. The CM was collected by centrifugation for 5 min at 1,500 rpm and was centrifuged again for 3 min at 3,000 rpm to remove cell debris. We used the SHED-CM without either enrichment or dilution. The CM was collected and stored at 4°C or −80°C before use in the following experiments.

SC migration study

SCs (cell line RT4-D6P2T) were purchased from American Type Culture Collection (ATCC, Manassas, VA). Transwell chambers with 8-μm pore filters (BD BioCoat Control Inserts; Becton Dickinson and Co., Franklin Lake, NJ) were used for migration analysis. A total of 1.0×10^5 SCs in 0.25% FBS-DMEM were added to the uncoated top chamber and SHED-CM was added to the lower chamber. Cell migration in the presence of 15% FBS and serum-free DMEM [DMEM (−)] served as the positive and negative controls, respectively. Cells were incubated at 37°C in 5% CO_2/95% air for 48 h. The upper sides of the filters were carefully rinsed with phosphate-buffered saline (PBS), and cells retained on the upper surfaces of the filters were removed with a swab. The Transwell filters were then stained with hematoxylin, removed with a scalpel, and mounted onto glass slides with the lower surface facing upward. The total numbers of migrated cells were counted using a light microscope (CK40; Olympus, Tokyo, Japan) at 200× magnification.

SC proliferation study

To test whether SHED-CM could enhance SC proliferation, we performed a 3-(4,5-dimethylthiazol-2-yl)-2,5-diphenyltetrazolium bromide (MTT) assay. Accordingly, 5.0×10^3 SCs were added to DMEM supplemented with 5% FBS and antibiotic–antimycotic solution and incubated for 24 h at 37°C in 5% CO_2/95% air. Subsequently, the medium was removed upon process extension from SCs and 100 μL of SHED-CM or presence of 15% FBS or DMEM (−) was added to the cells. The cells were incubated for 48 h at 37°C in 5% CO_2/95% air. Next, the MTT assay was performed by incubating the cells in

a 0.2% MTT solution (Cell Counting Kit; Dojindo Molecular Technologies, Kumamoto, Japan) at 37°C for 4 h. The absorbance was measured at 450 nm with a microplate reader (PowerScan4; DS Pharma Biomedical, Osaka, Japan).

Enzyme-linked immunosorbent assay

SHED-CM was subjected to enzyme-linked immunosorbent assay (ELISA) to determine the concentrations of nerve growth factor (NGF), brain-derived neurotrophic factor (BDNF), neurotrophin-3 (NT-3), glial cell line-derived neurotrophic factor (GDNF), ciliary neurotrophic factor (CNTF), vascular endothelial growth factor (VEGF), and hepatocyte growth factor (HGF). The concentrations of these factors were measured with human ELISA kits [BDNF, CNTF, VEGF, HGF (R&D Systems, Minneapolis MN), NGF, NT-3 (RayBiotech, Norcross, GA), GDNF (Abcam, Cambridge, MA)], according to the manufacturers' instructions. Experiments were performed in triplicate and absorbance was measured at 450 nm with a microplate reader (PowerScan4).

Real-time reverse transcriptase–polymerase chain reaction analysis

SCs were cultured with SHED-CM or DMEM (−) for 48 h. Total RNA was extracted with the RNeasy Mini Kit (Qiagen GmbH, Hilden, Germany), according to the manufacturer's protocol. The sequences of the specific primers and probes used for the real-time reverse transcriptase–polymerase chain reaction (RT-PCR) analysis of *NGF*, *BDNF*, *NT-3*, *CNTF*, *GDNF*, *VEGF*, *laminin*, *fibronectin*, *collagen type IV*, and *GAPDH* expression are listed in Table 1. Real-time RT-PCR analysis was performed with TaqMan Fast Virus 1-Step Master Mix (Applied Biosystems, Foster City, CA) on a 7000 Sequence Detector (PerkinElmer, Waltham, MA). Signals were analyzed using Sequence Detector software, version 1.1 (PerkinElmer). The PCR conditions were as follows: one cycle at 50°C for 5 min (reverse transcription), one cycle at 95°C for 20 s (inactivation/initial denaturation), and 40 cycles at 95°C for 15 s and 60°C for 60 s (amplification). The relative amount of each mRNA per sample was obtained by calculating respective standard curves. The standard curves for each mRNA were calculated using different concentrations (2,000, 400, 80, 16, and 3.2 ng) of total SC RNA. The relative expression levels were normalized to GAPDH expression levels.

Tube formation assay

An angiogenesis assay kit (Kurabo, Osaka, Japan) was used as described previously [42]. Human umbilical vein endothelial cells (HUVECs) and human diploid fibroblasts were mixed and seeded into the individual culture wells of a 24-well plate under optimal tubule formation conditions. Endothelial cell medium (EM) (Kurabo) containing VEGF (10 ng/mL; R&D Systems), HGF (10 ng/mL; R&D Systems), or SHED-CM was replaced on days 1, 4, 7, and 9. After 11 days, the plates were washed with PBS and fixed with 70% ethanol. After rinsing with PBS, the cells were incubated with primary antibody

Table 1. Primer Sequences Used for Real-Time Reverse Transcriptase–Polymerase Chain Reaction

Gene	*Sequence*	*Accession no.*
NGF	F: GTTGGAGATAAGACCACA R: CACTGTTGTTAATGTTCAC Probe: CCAGCACTGTCACCTCCTTG	XM_227525
BDNF	F: GCCCTTACTATGGATAGC R: CAGTGTACATACACAGGAA Probe: TCTATCCTTATGAACCGCCAGCC	NM_012513
NT-3	F: GGAAGATTATGTGGGCAA R: GGTGACTCTTATGCTCTG Probe: TAACCAATAGAACATCACCACGGAGG	NM_031073
CNTF	F: CTAGCAAGGAAGATTCGTTC R: CACTGAGTCAAGGTTGATA Probe: CCTGACTGCTCTTATGGAATCTTATGT	NM_013166
GDNF	F: CGTCTTAACTGCAATACAC R: GAACCGCTACAATATCGA Probe: TCAGTTCCTCCTTGGTTTCGTAGC	NM_019139
Laminin	F: GGCTTTTGACATCACTTA R: CGCTTATAAATGGCGAAA Probe: CGTCTCAAGTTCCACACCAGC	NM_053966
Fibronectin	F: GGTCACCTACAACATCATA R: CAGTGTTGCCTACAGTAA Probe: CTCTTCTCGGACCTTGTGCCT	NM_019143
Collagen IV	F: TGGCTTCAAAGGTGATAA R: GAACCTTTATCACCAGTG Probe: TTTGTCCTTTCTCTCCCTGGTCTC	NM_001135009
VEGF	F: ATCCCGGTTTAAATCCTG R: GGAACATTTACACGTCTG Probe: CACTGTGAGCCTTGTTCAGAGC	NM_031836
GAPDH	F: GTTCCAGTATGACTCTACC R: TCACCCCATTTGATGTTA Probe: TTCAACGGCACAGTCAAGC	NM_017008

(mouse anti-human CD31, 1:400; Kurabo) for 1 h at 37°C, followed by a secondary antibody (goat anti-mouse IgG alkaline phosphatase-conjugated antibody, 1:500; Kurabo) for 1 h at 37°C. The reaction yielded 5-bromo-4-chloro-3-indolyl phosphate/nitro blue tetrazolium. Total tube lengths and numbers of capillary connections (joints) in five different fields (5.5 mm^2 per field) per well were measured quantitatively using the Angiogenesis Image Analyzer, version 2 (Kurabo), and the results were subjected to statistical analysis.

DRG neurite growth assay and cell viability assay

DRG neurons were harvested from 3-day-old Wistar/ST rats using a previously described protocol [43–45]. Neurons were resuspended in neurobasal medium (Gibco) containing 2 mM L-glutamine (Gibco), 2% B27 (Gibco), and antibiotic–antimycotic solution, and then seeded onto poly-D-lysine/laminin-coated 24-well plates at a density of 400–500 neurons per well. DRG neurons were incubated with SHED-CM or DMEM (–) for 48 h. The neurons were then fixed in 4% paraformaldehyde for 15 min and incubated with a primary antibody against monoclonal β-III-tubulin (1:500; Sigma-Aldrich, St. Louis, MO) overnight at 4°C, followed by incubation with an Alexa Fluor 633-conjugated anti-mouse IgG secondary antibody (1:500; Invitrogen, Carlsbad, CA) for 1 h at room temperature. The stained neurons were examined under a fluorescence microscope (BZ9000; Keyence, Osaka, Japan). The average neurite length was quantitatively analyzed using BZ9000 analysis software (Keyence). A CCK-8 assay was performed to assess cell viability. Absorbance was measured at 450 nm using a microplate reader (PowerScan4).

Sciatic nerve transection and implantation

Male Wistar/ST rats weighing 250–300 g (7–8 weeks old) were anesthetized using pentobarbital (20 mg/kg intraperitoneally; Kyoritsu Seiyaku, Tokyo, Japan). The left sciatic nerves were carefully exposed and isolated at the mid-thigh level. Using a microscope and microsurgical instruments, a 12-mm segment of the nerve was excised and the nerve stumps were pulled 1 mm inside each end of the 12-mm silicone conduit (1.6 mm inner diameter) and secured to the epineurium with 8–0 nylon sutures (Natsume, Tokyo, Japan; Fig. 5A). The muscle and skin layers were closed with 4–0 Vicryl sutures (Ethicon Inc., Somerville, NJ). The animals were randomly assigned to the following five groups: (1) Sham: sciatic nerve exposure without any damage to the nerve tissue; (2) Transection: unrepaired sciatic nerve defects; (3) DMEM (–): DMEM (–)-filled silicon conduit; (4) SHED-CM: SHED-CM-filled silicon conduit; and (5) Autograft: the removed nerve segment was rotated 180° and reimplanted. After the surgery, the rats were placed under a warm plate until they awoke and were subsequently housed at a constant temperature (23°C ± 2°C) and humidity (55% ± 10%) under a 12-h light: 12-h dark cycle in cages with free access to food and water. We regularly observed the animals' health statuses. All experiments were performed with the minimum number of animals.

Walking track analysis

Functional recovery of the rats following sciatic nerve injury was assessed in a walking track analysis that was performed 3, 6, 9, and 12 weeks after surgery.

The distances from the heel to the top of the third toe (print length, PL), between the first and fifth toes (toe spread, TS) and between the second and fourth toes (intermediary toe spread, IT) were measured on both the experimental side (E) and contralateral normal side (N). The sciatic functional index (SFI) was calculated using the following formula [46]:

$$SFI = -38.3\ (EPL - NPL)/NPL + 109.5\ (ETS - NTS)/NTS + 13.3\ (EIT - NIT)/NIT - 8.8.$$

Two examiners blinded to the experimental repair conditions performed all of the animal evaluations. An SFI value near −100 indicates complete dysfunction, whereas a value near 0 indicates normal motor function [47].

Electrophysiologic testing

At 12 weeks after surgery, electromyography was performed to evaluate muscle activity in the leg affected by nerve injury. Under anesthesia, the sciatic nerve and gastrocnemius muscle on the injured side were exposed. Electrical stimuli were applied to the sciatic nerve and compound muscle action potentials (CMAPs) were recorded on the gastrocnemius muscle using PowerLab (AD Instruments, Nagoya, Japan). Digitalized data were stored on a computer and the latency, amplitude, and nerve conduction velocity of the CMPAs were calculated from these data.

Target muscle weight analysis and Masson's trichrome staining

Following electrophysiologic testing, the animals were sacrificed and the gastrocnemius muscles were dissected from the injured and normal sides and weighed. The gastrocnemius muscle wet weight ratio was calculated by comparing the weight of the gastrocnemius muscle on the injured side to that on the normal side. The gastrocnemius muscles were dissected from the mid-belly of the injured side. Muscle samples were fixed in 4% paraformaldehyde, embedded in paraffin, and cut vertically into 5-μm-thick sections. Masson's trichrome staining was performed to observe tissue morphology. The collagen fiber percentage was quantitatively analyzed using BZ-9000 analysis software (Keyence). We randomly selected three separate fields per slice for recording and analysis.

Histomorphological analysis

At 12 weeks after surgery, distal regenerating nerve segments were harvested and fixed in 2.5% glutaraldehyde solution (TAAB Laboratories Equipment Ltd., Reading, Berkshire, United Kingdom). The nerve segments were subsequently fixed in 2% osmium tetroxide (OsO_4) (TAAB Laboratories Equipment Ltd.) for 1 h, separately dehydrated in an ethanol gradient (50%, 70%, 80%, 90%, 95%, and 100%), and treated in a gradient of EPON812 (33%, 50%, 66%, and 100%; TAAB Laboratories Equipment Ltd.) in propylene oxide (Nacalai Tesque, Inc., Kyoto, Japan). Tissues were embedded in EPON812 in a 60°C oven for 48 h. Semithin sections (1 μm) were cut vertically with an ultramicrotome (Ultracut S; Leica Microsystems, Wetzlar, Germany) and stained with 0.3% toluidine blue solution. The number of myelinated axons was counted using a fluorescent microscope (BZ9000; Keyence). Ultrathin sections (70–80 nm) were cut with an ultramicrotome. The sections were

next placed on a copper mesh (150 mesh) and stained with lead citrate (Sigma-Aldrich) and 2% uranyl acetate. The stained samples were observed under a transmission electron microscope (TEM; JEM-1400EX; JEOL Ltd., Tokyo, Japan). We randomly selected five separate fields per slice for recording and analysis.

Statistical analyses

All histological and functional analyses were performed by observers blinded to each group. Data are expressed as mean ± standard deviation (SD). Statistical differences were evaluated using Tukey's honestly significant difference (HSD) test. Statistical significance was accepted at a P value of <0.05.

Results

SHED-CM enhances SC migration and proliferation

A Transwell assay was used to explore the effect of SHED-CM on SC migration in vitro. The numbers of SCs that migrated in DMEM (–), SHED-CM, and 15% FBS were 6.9 ± 2.8, 51.3 ± 8.2, and 81.4 ± 17, respectively. SHED-CM increased the SC migration rate by sevenfold in comparison with the negative control (*$P<0.05$; Fig. 1A).

MTT assays were performed to confirm that SHED-CM enhanced SC proliferation. SHED-CM significantly increased the SC proliferation rate when compared with DMEM (–) (*$P<0.05$; Fig. 1B).

Growth factors present in SHED-CM

The concentrations of growth factors, such as NGF, BDNF, NT-3, GDNF, CNTF, VEGF, and HGF in SHED-CM, were quantified through ELISA. These factors were not detected in DMEM (–), whereas SHED-CM contained NGF, BDNF, NT-3, GDNF, CNTF, VEGF, and HGF at respective concentrations of 58.7 ± 28, 46.4 ± 5.3, 24.9 ± 2.1, 115 ± 50, 131 ± 71, 556 ± 65, and 3,350 ± 560 pg/mL (Table 2).

SHED-CM enhances the expression of NTF, angiogenic molecule, and ECM marker genes

The effects of SHED-CM and DMEM (–) on SC gene expression were measured using real-time RT-PCR analysis. The expression levels of genes encoding NTFs (*NGF*, *BDNF*, *NT-3*, *CNTF*, *GDNF*), angiogenic molecules (*VEGF*), and ECM molecules *(laminin, fibronectin, collagen type IV)* were significantly upregulated in SCs cultured with SHED-CM relative to those cultured with DMEM (–) (*$P<0.05$; Fig. 2).

SHED-CM stimulates neurite outgrowth from and increases the viability of DRG neurons

To determine the effects of SHED-CM on neuritogenesis, a neurite outgrowth assay was performed. DRG neurons were treated with SHED-CM or DMEM (–) for 48 h and subsequently immunostained with a β-III-tubulin antibody to measure neuritis. The average neurite outgrowth (μm) was significantly greater in neurons treated with SHED-CM than in those treated with DMEM (–) (*$P<0.05$; Fig. 3B).

To compare the cell viabilities of DRG neurons cultured with SHED-CM and DMEM (–), CCK8 assays were performed. SHED-CM significantly increased the viability of DRG neurons relative to DMEM (–) (*$P<0.05$; Fig. 3C).

SHED-CM stimulates angiogenesis in vitro

To determine the effect of SHED-CM on angiogenesis, a tube formation assay was performed. HUVECs seeded in EM did not exhibit tube formation. In contrast, HUVECs exposed to SHED-CM, VEGF, or HGF exhibited noticeable increases in length. Quantification of tube length yielded values of 3,026 ± 690 pixels with EM, 9,723 ± 97 pixels with SHED-CM, 13,200 ± 386 pixels with VEGF, and 15,135 ± 972 pixels with HGF. The respective numbers of joints were 13 ± 5.3, 42 ± 4.3, 69.3 ± 4.2, and 62.3 ± 4.9. HUVECs cultured in SHED-CM exhibited significant increases in tube length and joint number (*$P<0.05$; Fig. 4B, C).

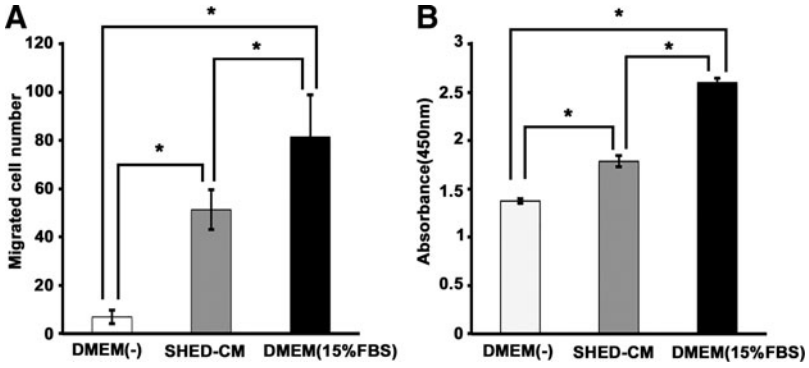

FIG. 1. Effects of SHED-CM on SC migration and proliferation. **(A)** Transwell migration assay. The migration of SCs cultured in SHED-CM was enhanced relative to those cultured in DMEM (–). DMEM (–), SHED-CM, DMEM (15% FBS): $n=5$ per group. Data are shown as mean ± SD. *$P<0.05$. **(B)** Cell proliferation assay. SC proliferation is reported as the absorbance at 450 nm following MTT analysis. The proliferation of SCs cultured in SHED-CM was also enhanced relative to those cultured in DMEM (–). Cells cultured in DMEM (15% FBS) were used as a positive control. DMEM (–), SHED-CM, DMEM (15% FBS): $n=5$ per group. Data are shown as mean ± SD. *$P<0.05$. SHED, stem cells from human exfoliated deciduous teeth; SHED-CM, serum-free conditioned media from SHEDs; SC, Schwann cell; DMEM, Dulbecco's modified Eagle's medium; FBS, fetal bovine serum.

Table 2. Concentrations of Growth Factors in SHED-CM (pg/mL)

Factors	*Concentrations (pg/mL)*
NGF	58.7 ± 28
BDNF	46.4 ± 5.3
NT-3	24.9 ± 2.1
GDNF	115 ± 50
CNTF	131 ± 71
VEGF	556 ± 65
HGF	3350 ± 560

BDNF, brain-derived neurotrophic factor; CNTF, ciliary neurotrophic factor; GDNF, glial cell line-derived neurotrophic factor; HGF, hepatocyte growth factor; NGF, nerve growth factor; NT-3, neurotrophin-3; VEGF, vascular endothelial growth factor.

SHED-CM enhances nerve regeneration

Not all sciatic nerves regenerated in the Transection group at 12 weeks after surgery. The ends of these non-regenerated nerves formed neuromas. Neither dislocation of the grafts nor formation of neuromas was evident after 12 weeks after surgery. The diameters of regenerated nerves in SHED-CM-treated rats were thicker than those in DMEM (–)-treated rats (Fig. 5B).

SHED-CM enhances axon regeneration and remyelination

At 12 weeks after surgery, regenerated myelinated nerve fibers were observed at the distal portion of the injured nerve using toluidine blue staining and TEM. Toluidine blue staining revealed nerve fibers of different sizes and numbers in each group. Obviously, SHED-CM more strongly promoted nerve regeneration relative to DMEM (–). The number of regenerated myelinated nerve fibers was significantly higher in the SHED-CM and Autograft groups compared with the DMEM (–) group ($*P < 0.05$; Fig. 6C). TEM images showed that the regenerated axons consisted of rounded myelin sheaths in each group. The mean G-ratios for the Sham, DMEM (–), SHED-CM, and Autograft groups were 0.64 ± 0.02, 0.79 ± 0.02, 0.74 ± 0.01, and 0.71 ± 0.02, respectively. The degree of myelination was significantly higher in the SHED-CM and Autograft groups than in the DMEM (–) group ($*P < 0.05$; Fig. 6D).

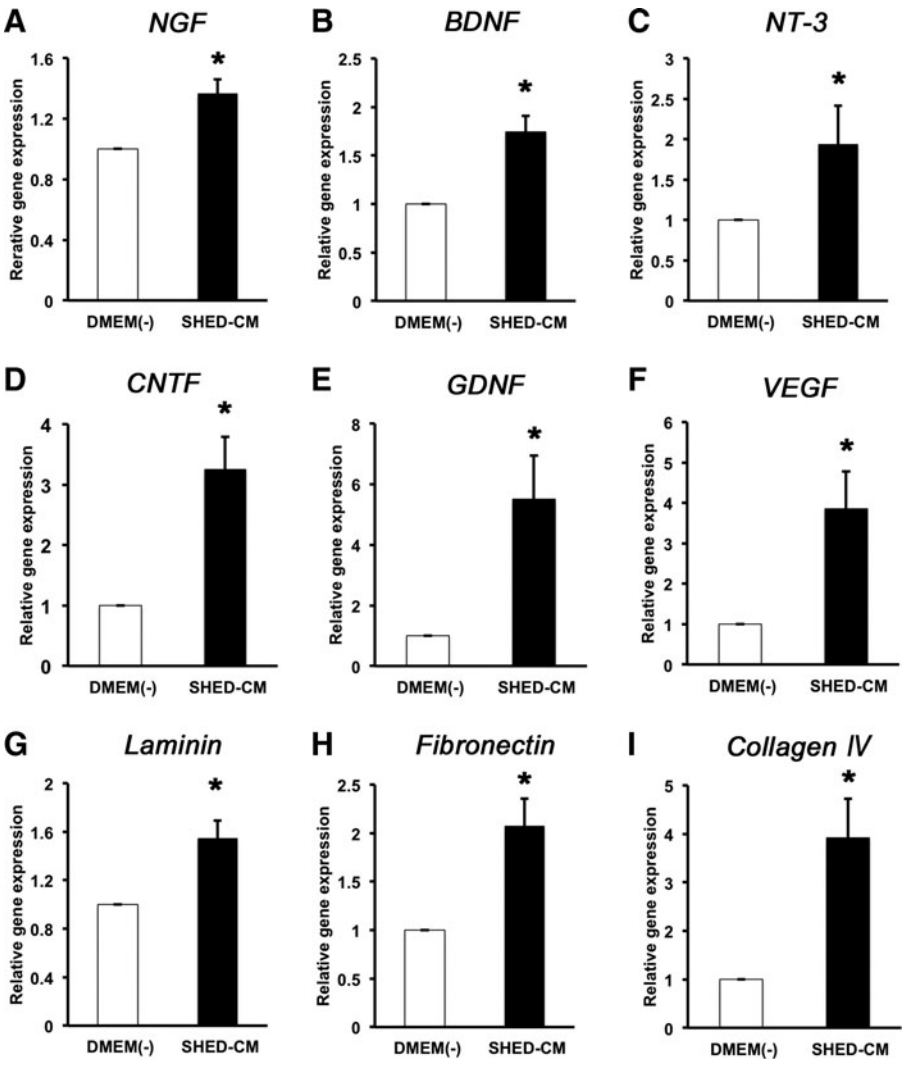

FIG. 2. Effect of SHED-CM on SC gene expression. The mRNA levels of **(A)** *NGF*, **(B)** *BDNF*, **(C)** *NT-3*, **(D)** *CNTF*, **(E)** *GDNF*, **(F)** *VEGF*, **(G)** *laminin*, **(H)** *fibronectin*, and **(I)** *collagen IV* were analyzed in SCs cultured with SHED-CM or DMEM (–) using real-time RT-PCR. The expression levels of NTF-, angiogenic molecule-, and ECM molecule-encoding genes were upregulated in SCs cultured with SHED-CM relative to those cultured with DMEM (–). DMEM (–), SHED-CM: $n = 5$ per group. Data are shown as mean ± SD. $*P < 0.05$. ECM, extracellular matrix; NTF, neurotrophic factor; RT-PCR, reverse transcriptase–polymerase chain reaction.

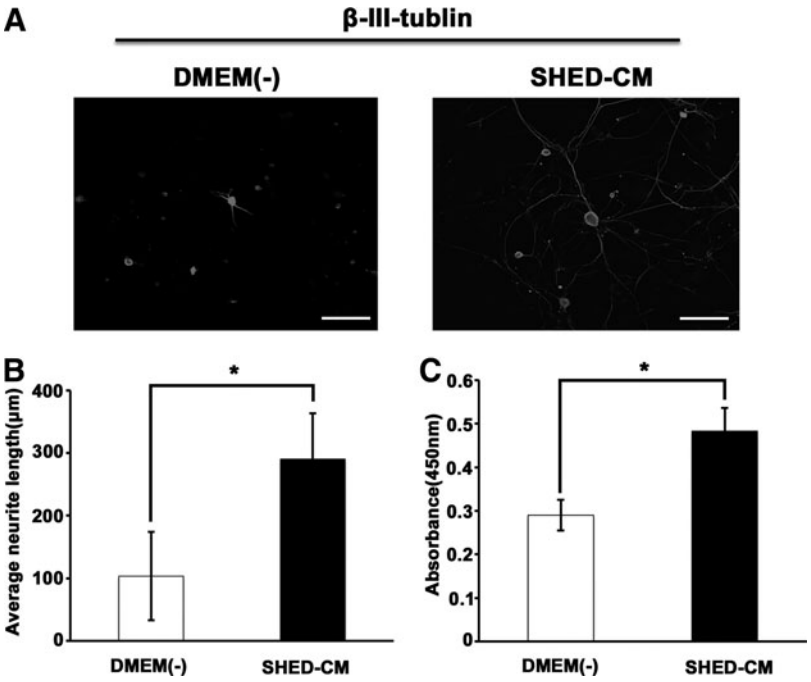

FIG. 3. Effects of SHED-CM on DRG neuronal outgrowth and survival. **(A)** β-III-tubulin immunostaining of DRG neurons cultured with SHED-CM or DMEM (–) for 48 h. Scale bar = 100 μm. **(B)** Quantitative analysis of average neurite length. The average neurite outgrowth was significantly higher in neurons treated with SHED-CM than in those treated with DMEM (–). DMEM (–), SHED-CM: $n = 5$ per group. Data are shown as mean ± SD. $^*P < 0.05$. **(C)** DRG neuron viability. Cell viability is reported as the absorbance at 450 nm following CCK-8 assay. Compared with DMEM (–), SHED-CM significantly increased the viability of DRG neurons. DMEM (–), SHED-CM: $n = 5$ per group. Data are shown as mean ± SD. $^*P < 0.05$. DRG, dorsal root ganglion.

SHED-CM improves motor function recovery

We assessed motor function recovery using a walking track analysis (SFI) and electrophysiologic evaluation. Negative control animals, in which a critical sciatic nerve defect was induced without repair, exhibited SFI values near −100 throughout the 12-week period. Therefore, motor function was not recovered in the Transection group. The lowest SFI values in the DMEM (–), SHED-CM, and Autograft groups were detected immediately after nerve injury and subsequently exhibited time-dependent increases. The SFI value at 12 weeks postrepair was significantly higher in the SHED-CM and Autograft groups than in the DMEM (–) group ($^*P < 0.05$; Fig. 7A).

CMAP values were measured on the injured side at 12 weeks after surgery. CMAPs were not detected in the Transection group. CMAP recordings demonstrated the

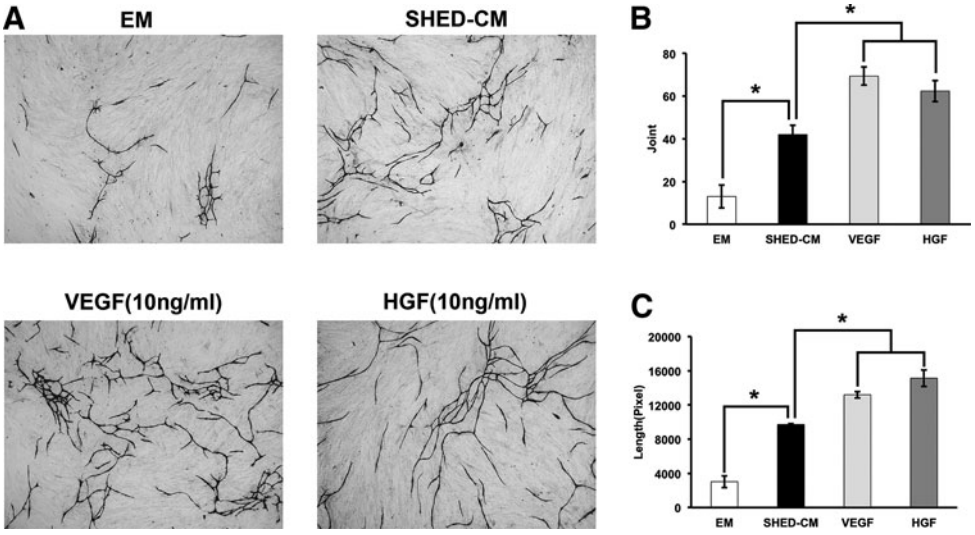

FIG. 4. Effect of SHED-CM on capillary tube-like HUVEC formation. **(A)** HUVECs were cultured with EM, SHED-CM, VEGF (10 ng/mL), and HGF (10 ng/mL). After 11 days, capillary tube-like structures were observed. Scale bar = 100 μm. **(B)** Statistical analysis of the total blood vessel lengths. HUVECs cultured in SHED-CM exhibited significant increases in tube length when compared with cells cultured in DMEM (–). EM, SHED-CM, VEGF, HGF: $n = 3$ per group. Data are shown as mean ± SD. $^*P < 0.05$. **(C)** Statistical analysis of the numbers of joints. HUVECs cultured in SHED-CM exhibited significantly higher numbers of joints when compared with cells cultured in DMEM (–). EM, SHED-CM, VEGF, HGF: $n = 3$ per group. Data are shown as mean ± SD. $^*P < 0.05$. EM, endothelial cell medium; HGF, hepatocyte growth factor; HUVEC, human umbilical vein endothelial cells; VEGF, vascular endothelial growth factor.

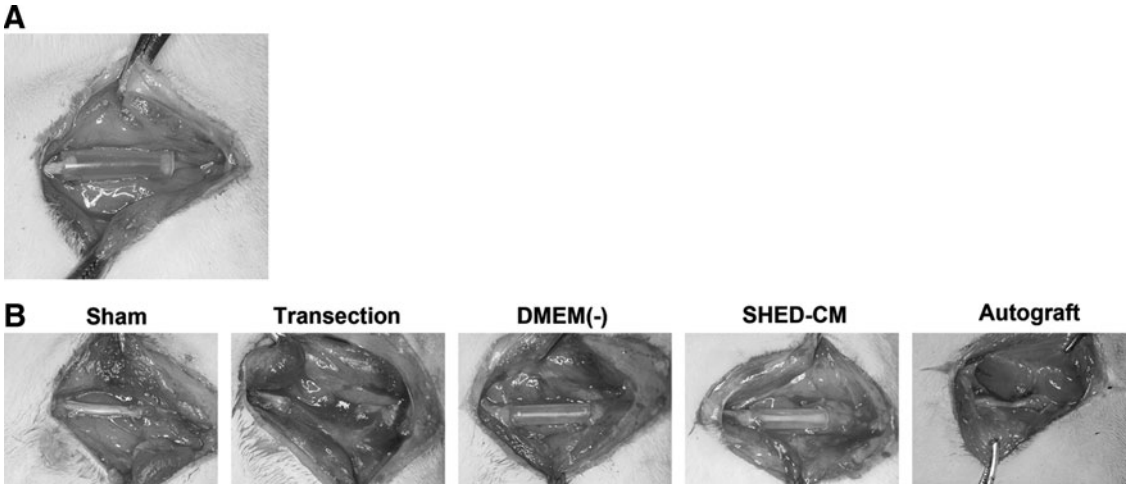

FIG. 5. Regeneration in a sciatic nerve transection rat model. **(A)** The sciatic nerve was transected to leave a 10 mm length and was bridged with a silicon conduit. **(B)** Microscopic view of the regenerated nerves 12 weeks after surgery. Images are representatives of the following groups: Sham, Transection, DMEM (−), SHED-CM, and Autograft. The diameters of regenerated nerves were thicker in rats treated with SHED-CM relative to rats treated with DMEM (−).

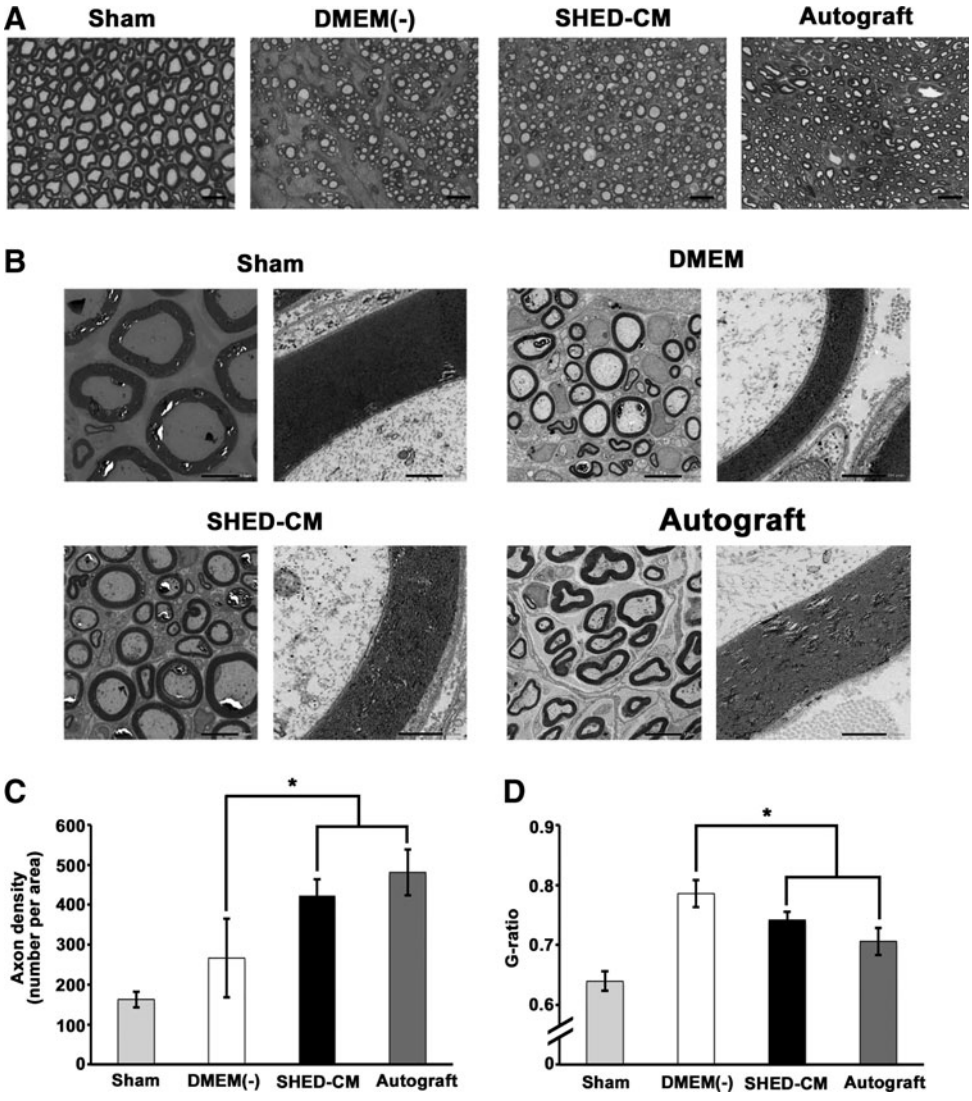

FIG. 6. Myelin sheath morphology in the regenerated nerves. **(A)** Toluidine blue staining of semi-thin cross sections from the distal portions of regenerated nerves at 12 weeks after surgery. Scale bar = 20 μm. **(B)** TEM images of ultrathin cross sections of the distal regenerated nerves at 12 weeks after surgery. Scale bars = 5.0 μm, 500 nm. **(C)** Densities of remyelinated axons in the distal nerve portions. The number of regenerated myelinated fibers was significantly higher in the SHED-CM and Autograft groups than in the DMEM (−) group. Sham, DMEM (−), SHED-CM, Autograft: $n = 4$ per group. Data are shown as mean ± SD. $^*P < 0.05$. **(D)** Statistical analysis of the G-ratios. The G-ratio was significantly improved in the SHED-CM group relative to the DMEM (−) group. Sham, DMEM (−), SHED-CM, Autograft: $n = 4$ per group. Data are shown as mean ± SD. $^*P < 0.05$. TEM, transmission electron microscope.

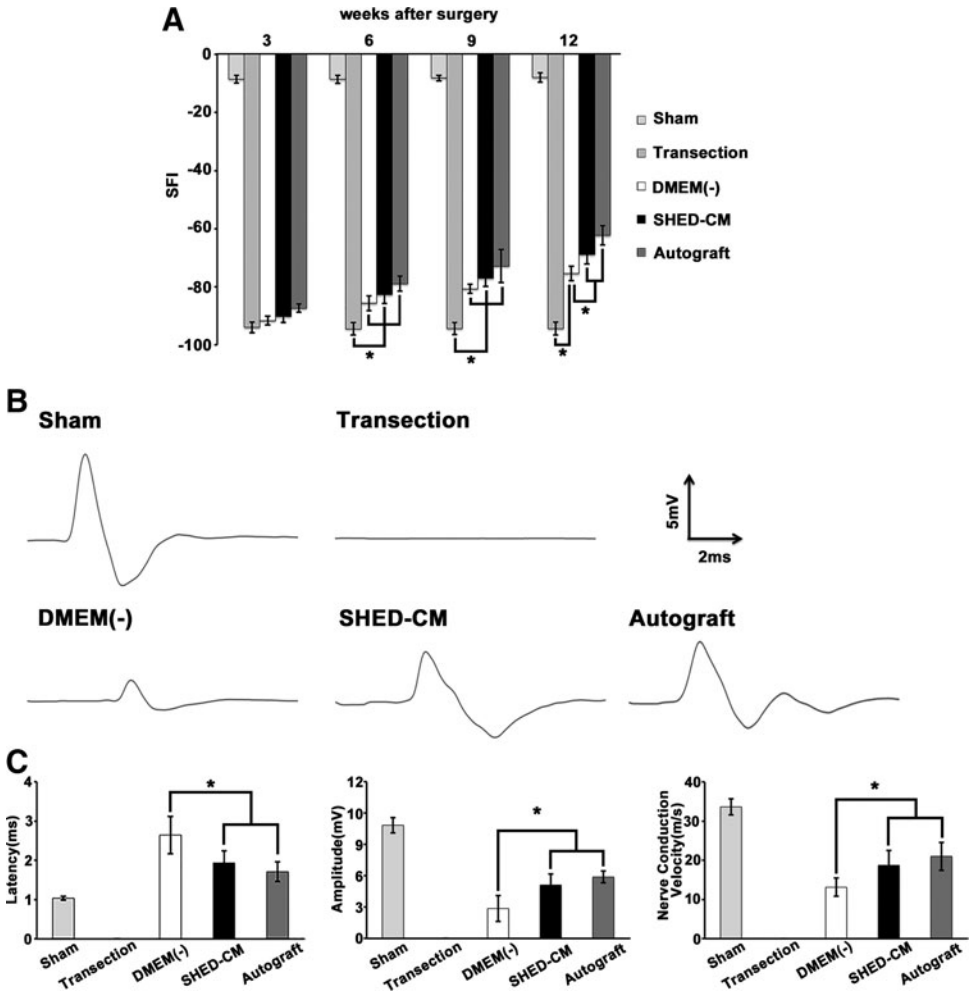

FIG. 7. Motor function recovery after sciatic nerve transaction. **(A)** The SFI was analyzed to assess motor function at 3, 6, 9, and 12 weeks after surgery. The SFI at 12 weeks after repair was significantly higher in the SHED-CM and Autograft groups than in the DMEM (–) group. Sham, Transection, DMEM (–), SHED-CM, Autograft: $n = 6$ per group. Data are shown as mean ± SD. $^*P < 0.05$. **(B)** Representative CMAP recordings of the injured side at 12 weeks after surgery. **(C)** Histograms show the peak CMAP amplitude, latency, and nerve conduction velocity. Sham, Transection, DMEM (–), SHED-CM, Autograft: $n = 6$ per group. Data are shown as mean ± SD. $^*P < 0.05$. CMAP, compound muscle action potential; SFI, sciatic functional index.

recovery of electrophysiologic properties in the SHED-CM, DMEM (–), and Autograft groups. The detected CMAP amplitude was significantly higher in the SHED-CM and Autograft groups than in the DMEM (–) group at 12 weeks after surgery. However, the CMAP amplitude of the Sham group was significantly higher compared with other groups. The differences among nerve conduction velocities were similar to those among CMAP values. In addition, the latency values in the SHED-CM and Autograft groups were significantly longer than that measured in the Sham group, but shorter than that in the DMEM (–) group ($^*P < 0.05$; Fig. 7B, C).

SHED-CM prevents muscle atrophy and maintains muscle fibers

The gastrocnemius muscles atrophied after nerve transection and subsequently regained innervation after nerve regeneration. In the Transection group, the muscles exhibited a slim gross morphology. The gastrocnemius muscle wet weight was relatively higher in the reinnervated muscle of the SHED-CM and Autograft groups when compared with that of the DMEM (–) group ($^*P < 0.05$; Fig. 8C). Masson's trichrome staining was performed to examine the rat gastrocnemius muscle morphology. The collagen fiber percentage was significantly lower in the SHED-CM and Autograft groups than in the DMEM (–) group ($^*P < 0.05$; Fig. 8D). The gastrocnemius muscle wet weight ratios and collagen fiber percentages of the DMEM (–), SHED-CM, and Autograft groups were improved relative to those of the Transection group.

Discussion

Our findings suggest that SHED-CM contains various cytokines and chemokines that can enhance peripheral nerve regeneration through complicated processes. Recently, many types of biomaterial and stem cell transplantation therapy have been proposed to enhance peripheral nerve regeneration and functional recovery. Some studies have reported that transplanted stem cells could promote peripheral nerve regeneration through host cell replacement, cell differentiation, or cell-to-cell contact-mediated signaling. However, transplanted stem cells exhibit poor differentiation and survival [12,48]. Therefore, a paracrine mechanism triggered by growth factors and cytokines secreted by transplanted stem cells has been suggested to enhance peripheral nerve regeneration [49].

Recent studies have described the secretion of various growth factors and cytokines from stem cells. In our previous study, microarray analysis of SHEDs revealed high expression levels of several growth factors, such as transforming growth factor, connective tissue growth factor, and NTFs [50]. We showed that SHED-CM contained NGF,

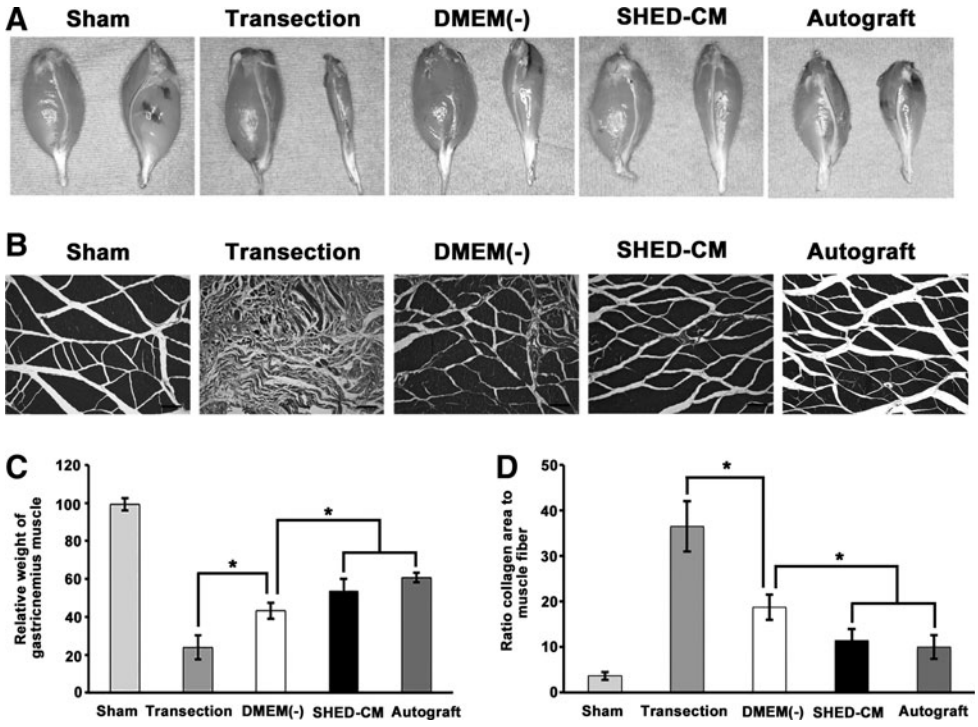

FIG. 8. Muscle wet weight and morphological analysis. **(A)** Macroscopic view of the gastrocnemius muscles of both hind limbs at 12 weeks after surgery. **(B)** Masson's trichrome staining of gastrocnemius muscle cross sections. **(C)** Statistical analysis of the gastrocnemius muscle wet weight ratios. The relative gastrocnemius muscle was greater in the SHED-CM and Autograft groups than in the DMEM (−) group. Sham, Transection, DMEM (−), SHED-CM, Autograft: $n = 6$ per group. Data are shown as mean ± SD. $^*P < 0.05$. **(D)** Histograms show the average collagen fiber areas. The collagen fiber percentage was significantly lower in the SHED-CM and Autograft groups relative to the DMEM (−) group. Sham, Transection, DMEM (−), SHED-CM, Autograft: $n = 6$ per group. Data are shown as mean ± SD. $^*P < 0.05$.

BDNF, NT-3, CNTF, GDNF, VEGF, and HGF (Table 2). These factors were found to enhance peripheral nerve regeneration in previous studies. In addition, macrophage accumulation was reported to increase dramatically following bone marrow stem cell transplantation [12] as stem cells, including SHEDs, secrete monocyte chemotactic protein-1. Therefore, the accumulation of macrophages at an early stage after PNI accelerates debris removal increases the concentrations of growth factors and promotes the migration of SCs. After PNI, SCs proliferate and migrate from degenerating axons to form a microenvironment supportive of axonal regeneration [7]. Therefore, peripheral nerve regeneration requires the recruitment of SCs into the nerve conduit where these cells produce a range of NTFs, cytokines, and ECM and adhesion molecules to promote axonal regeneration. Yang et al. reported that bone marrow-derived mesenchymal stem cell CM encouraged SC proliferation through the mitogen-activated protein kinase pathway [51]. Our results showed that SHED-CM enhanced both migration and proliferation in vitro (Fig. 1). This indicates that SHED-CM contains factors that can regulate the mobilization of SCs to the target tissue. Our real-time RT-PCR results revealed that the expression of NTFs, such as *NGF*, *BDNF*, *NT-3*, *CNTF*, and *GDNF*, was significantly upregulated in SCs cultured with SHED-CM versus DMEM (−) (Fig. 2A–E). NTFs regulate SC proliferation and migration and support survival, maintenance, and axonal elongation [15]. The efficacy of NTFs has been investigated in peripheral nerve regeneration studies. In sensory neurons, NGF promotes primary survival and axonal outgrowth [52,53]. BDNF promotes motor neuron survival and differentiation [54,55]. NT-3 supports myelin formation by enhancing SC motility and migration [56,57]. CNTF is a neuroprotective agent that facilitates remyelination [58,59]. GDNF enhances motor and sensory nerve regeneration [60,61]. The application of multiple rather than single factors holds great therapeutic promise. For example, a combination of BDNF and CNTF significantly improved functional recovery versus single-factor treatments in a severed sciatic nerve rat model [62]. The concentrations of these factors in SHED-CM may be low. However, multiple factors secreted from SHEDs may act in a synergistic or additive manner to enhance peripheral nerve regeneration.

In the present study, we examined the hypothesis that SHED-CM enhances axonal regeneration and protects neurons in a sciatic nerve transection rat model. We demonstrated that SHED-CM enhanced neurite outgrowth and neuronal cell survival (Fig. 3B, C) in vitro. The electrophysiological and morphological analyses conducted at 12 weeks after surgery allowed evaluation of the regenerative nerve outcomes. The results revealed significantly better nerve regeneration in the SHED-CM group than in the DMEM (−) group (Figs. 5 and 6). Based on these results, SHED-CM enhanced axonal regeneration. Functional recovery is the ultimate goal of PNI research. However, it is difficult to assess neurological functional recovery directly in a rat model. Therefore, we assessed functional recovery using indirect methods such as the SFI value

and changes in target muscle weight. The SFI value at 12 weeks after surgery was significantly higher in the SHED-CM group than in the DMEM (–) group (Fig. 7A), suggesting improved sciatic nerve reinnervation of the target muscle and consequently better functional recovery. In addition, the SHED-CM group exhibited reduced target muscle atrophy when compared with the DMEM (–) group, which also suggested improved muscle function (Fig. 8). This regeneration may have been facilitated by an advantageous regenerative microenvironment and the secretion of cytokines, chemokines, and NTFs from SHEDs. Angiogenesis is an important process in tissue regeneration, including peripheral nerve regeneration. We demonstrated that SHED-CM could promote tube formation (Fig. 4) and the expression of the angiogenic molecule, *VEGF*, in SCs in vitro (Fig. 2F). Numerous studies have indicated that VEGF plays a pivotal role in promoting angiogenesis during tissue regeneration. VEGF promotes the migration and proliferation of vascular endothelial cells [63]. Recently, HGF has also been reported to promote angiogenesis [64]. Moreover, a combination of VEGF and HGF induces a more robust angiogenic response [65]. Our results demonstrated that paracrine factors released from SHEDs not only promoted angiogenesis directly but also enhanced the potential for angiogenesis in SCs. ECM consists of collagens, adhesive glycoproteins, and proteoglycans produced by resident cells in tissues or organs [66]. Cell adhesion to ECM enhances survival, differentiation, and migration [67]. ECM plays a prominent role in maintaining an advantageous microenvironment for tissue regeneration and providing a guide for axonal outgrowth toward the correct target [68]. In this study, the expression of *laminin*, *fibronectin*, and *collagen type IV* mRNA was significantly upregulated in SCs cultured in SHED-CM relative to those cultured in DMEM (–) (Fig. 2G–I). These results indicate that ECM derived from SCs in SHED-CM may enhance axonal outgrowth. In addition, multiple factors secreted from SHED may not only lead directly to peripheral nerve regeneration but might also influence SCs. Moreover, SHED-CM could provide an advantageous microenvironment for peripheral nerve regeneration.

In summary, we showed that SHED-CM could promote axonal regeneration and functional recovery in a sciatic nerve defect rat model. SHED-CM enhanced axon growth, peripheral nerve tissue angiogenesis, SC migration, proliferation, and activation, and neuron survival. Therefore, SHED-CM promotes peripheral nerve regeneration through various processes, leading to functional recovery. Our results suggest that SHED-CM is a potential promising strategy for clinical PNI treatment.

Acknowledgments

The authors are especially grateful to Dr. Hitoshi Hirata and Dr. Hideyuki Ota, Department of Hand Surgery, Nagoya University Graduate School of Medicine, for valuable discussion and technical instructions. The authors are grateful to Dr. Koji Itakura, Division for Medical Research Engineering, Nagoya University Graduate School of Medicine, for technical support and assistance and thank the members of the Department of Oral and Maxillofacial Surgery for their encouragement to complete this study. The authors would also like to thank the Division of Experimental and Medical Research Engineering, Nagoya University Graduate School of Medicine, for housing the animals.

Author Disclosure Statement

No competing financial interests exist.

References

1. Mokarram N, A Merchant, V Mukhatyar, G Patel and RV Bellamkonda. (2012). Effect of modulating macrophage phenotype on peripheral nerve repair. Biomaterials 33:8793–8801.
2. Pfister BJ, T Gordon, JR Loverde, AS Kochar, SE Mackinnon and DK Cullen. (2011). Biomedical engineering strategies for peripheral nerve repair: surgical applications, state of the art, and future challenges. Crit Rev Biomed Eng 39:81–124.
3. Pabari A, SY Yang, AM Seifalian and A Mosahebi. (2010). Modern surgical management of peripheral nerve gap. J Plast Reconstr Aesthet Surg 63:1941–1948.
4. Tang S, J Zhu, Y Xu, AP Xiang, MH Jiang and D Quan. (2013). The effects of gradients of nerve growth factor immobilized PCLA scaffolds on neurite outgrowth in vitro and peripheral nerve regeneration in rats. Biomaterials 34:7086–7096.
5. Lin MY, G Manzano and R Gupta. (2013). Nerve allografts and conduits in peripheral nerve repair. Hand Clin 29:331–348.
6. Mackinnon SE and AR Hudson. (1992). Clinical application of peripheral nerve transplantation. Plast Reconstr Surg 90:695–699.
7. Chen ZL, WM Yu and S Strickland. (2007). Peripheral regeneration. Annu Rev Neurosci 30:209–233.
8. Mokarram N and RV Bellamkonda. (2011). Overcoming endogenous constraints on neuronal regeneration. IEEE Trans Biomed Eng 58:1900–1906.
9. Gaudet AD, PG Popovich and MS Ramer. (2011). Wallerian degeneration: gaining perspective on inflammatory events after peripheral nerve injury. J Neuroinflammation 8:110.
10. Chaballe L, P Close, M Sempels, S Delstanche, J Fanielle, L Moons, P Carmeliet, J Schoenen, A Chariot and R Franzen. (2011). Involvement of placental growth factor in Wallerian degeneration. Glia 59:379–396.
11. Shen ZL, F Lassner, A Bader, M Becker, GF Walter and A Berger. (2000). Cellular activity of resident macrophages during Wallerian degeneration. Microsurgery 20:255–261.
12. Ribeiro-Resende VT, PM Pimentel-Coelho, LA Mesentier-Louro, RM Mendez, JP Mello-Silva, MC Cabral-da-Silva, FG de Mello, RA de Melo Reis and R Mendez-Otero. (2009). Trophic activity derived from bone marrow mononuclear cells increases peripheral nerve regeneration by acting on both neuronal and glial cell populations. Neuroscience 159:540–549.
13. Griffin JW, R George and T Ho. (1993). Macrophage systems in peripheral nerves. A review. J Neuropathol Exp Neurol 52:553–560.
14. Stoll G, JW Griffin, CY Li and BD Trapp. (1989). Wallerian degeneration in the peripheral nervous system: participation of both Schwann cells and macrophages in myelin degradation. J Neurocytol 18:671–683.
15. Madduri S and B Gander. (2010). Schwann cell delivery of neurotrophic factors for peripheral nerve regeneration. J Peripher Nerv Syst 15:93–103.
16. Dubovy P. (2004). Schwann cells and endoneurial extracellular matrix molecules as potential cues for sorting of regenerated axons: a review. Anat Sci Int 79:198–208.
17. Ding F, J Wu, Y Yang, W Hu, Q Zhu, X Tang, J Liu and X Gu. (2010). Use of tissue-engineered nerve grafts consisting of a chitosan/poly(lactic-co-glycolic acid)-based scaffold included with bone marrow mesenchymal cells for bridging 50-mm dog sciatic nerve gaps. Tissue Eng Part A 16:3779–3790.

18. Chen CJ, YC Ou, SL Liao, WY Chen, SY Chen, CW Wu, CC Wang, WY Wang, YS Huang and SH Hsu. (2007). Transplantation of bone marrow stromal cells for peripheral nerve repair. Exp Neurol 204:443–453.
19. Mohammadi R, S Azizi and K Amini. (2013). Effects of undifferentiated cultured omental adipose-derived stem cells on peripheral nerve regeneration. J Surg Res 180:e91–e97.
20. Gu JH, YH Ji, ES Dhong, DH Kim and ES Yoon. (2012). Transplantation of adipose derived stem cells for peripheral nerve regeneration in sciatic nerve defects of the rat. Curr Stem Cell Res Ther 7:347–355.
21. Lavasani M, SD Thompson, JB Pollett, A Usas, A Lu, DB Stolz, KA Clark, B Sun, B Peault and J Huard. (2014). Human muscle-derived stem/progenitor cells promote functional murine peripheral nerve regeneration. J Clin Invest 124:1745–1756.
22. Zeng X, L Zhang, L Sun, D Zhang, H Zhao, J Jia and W Wang. (2013). Recovery from rat sciatic nerve injury in vivo through the use of differentiated MDSCs in vitro. Exp Ther Med 5:193–196.
23. Sasaki R, S Aoki, M Yamato, H Uchiyama, K Wada, H Ogiuchi, T Okano and T Ando. (2011). PLGA artificial nerve conduits with dental pulp cells promote facial nerve regeneration. J Tissue Eng Regen Med 5:823–830.
24. Sasaki R, S Aoki, M Yamato, H Uchiyama, K Wada, T Okano and H Ogiuchi. (2008). Tubulation with dental pulp cells promotes facial nerve regeneration in rats. Tissue Eng Part A 14:1141–1147.
25. Ide C, Y Nakai, N Nakano, TB Seo, Y Yamada, K Endo, T Noda, F Saito, Y Suzuki, M Fukushima and T Nakatani. (2010). Bone marrow stromal cell transplantation for treatment of sub-acute spinal cord injury in the rat. Brain Res 1332:32–47.
26. Chen L, R Coleman, R Leang, H Tran, A Kopf, CM Walsh, I Sears-Kraxberger, O Steward, WB Macklin, JF Loring and TE Lane. (2014). Human neural precursor cells promote neurologic recovery in a viral model of multiple sclerosis. Stem Cell Reports 2:825–837.
27. Sowa Y, T Imura, T Numajiri, K Nishino and S Fushiki. (2012). Adipose-derived stem cells produce factors enhancing peripheral nerve regeneration: influence of age and anatomic site of origin. Stem Cells Dev 21:1852–1862.
28. Yew TL, YT Hung, HY Li, HW Chen, LL Chen, KS Tsai, SH Chiou, KC Chao, TF Huang, HL Chen and SC Hung. (2011). Enhancement of wound healing by human multipotent stromal cell conditioned medium: the paracrine factors and p38 MAPK activation. Cell Transplant 20:693–706.
29. Moon KM, YH Park, JS Lee, YB Chae, MM Kim, DS Kim, BW Kim, SW Nam and JH Lee. (2012). The effect of secretory factors of adipose-derived stem cells on human keratinocytes. Int J Mol Sci 13:1239–1257.
30. Bronckaers A, P Hilkens, Y Fanton, T Struys, P Gervois, C Politis, W Martens and I Lambrichts. (2013). Angiogenic properties of human dental pulp stem cells. PLoS One 8:e71104.
31. Yamagata M, A Yamamoto, E Kako, N Kaneko, K Matsubara, K Sakai, K Sawamoto and M Ueda. (2013). Human dental pulp-derived stem cells protect against hypoxic-ischemic brain injury in neonatal mice. Stroke 44:551–554.
32. Inoue T, M Sugiyama, H Hattori, H Wakita, T Wakabayashi and M Ueda. (2013). Stem cells from human exfoliated deciduous tooth-derived conditioned medium enhance recovery of focal cerebral ischemia in rats. Tissue Eng Part A 19:24–29.
33. Cantinieaux D, R Quertainmont, S Blacher, L Rossi, T Wanet, A Noel, G Brook, J Schoenen and R Franzen. (2013). Conditioned medium from bone marrow-derived mesenchymal stem cells improves recovery after spinal cord injury in rats: an original strategy to avoid cell transplantation. PLoS One 8:e69515.
34. Osugi M, W Katagiri, R Yoshimi, T Inukai, H Hibi and M Ueda. (2012). Conditioned media from mesenchymal stem cells enhanced bone regeneration in rat calvarial bone defects. Tissue Eng Part A 18:1479–1489.
35. Katagiri W, M Osugi, T Kawai and M Ueda. (2013). Novel cell-free regeneration of bone using stem cell-derived growth factors. Int J Oral Maxillofac Implants 28:1009–1016.
36. Inukai T, W Katagiri, R Yoshimi, M Osugi, T Kawai, H Hibi and M Ueda. (2013). Novel application of stem cell-derived factors for periodontal regeneration. Biochem Biophys Res Commun 430:763–768.
37. Kawai T, W Katagiri, M Osugi, Y Sugimura, H Hibi and M Ueda. (2015). Secretomes from bone marrow-derived mesenchymal stromal cells enhance periodontal tissue regeneration. Cytotherapy 17: 369–381.
38. Ogata K, W Katagiri, M Osugi, T Kawai, Y Sugimura, H Hibi, S Nakamura and M Ueda. (2015). Evaluation of the therapeutic effects of conditioned media from mesenchymal stem cells in a rat bisphosphonate-related osteonecrosis of the jaw-like model. Bone 74:95–105.
39. Gronthos S, J Brahim, W Li, LW Fisher, N Cherman, A Boyde, P DenBesten, PG Robey and S Shi. (2002). Stem cell properties of human dental pulp stem cells. J Dent Res 81:531–535.
40. Sakai K, A Yamamoto, K Matsubara, S Nakamura, M Naruse, M Yamagata, K Sakamoto, R Tauchi, N Wakao, et al. (2012). Human dental pulp-derived stem cells promote locomotor recovery after complete transection of the rat spinal cord by multiple neuro-regenerative mechanisms. J Clin Invest 122:80–90.
41. Miura M, S Gronthos, M Zhao, B Lu, LW Fisher, PG Robey and S Shi. (2003). SHED: stem cells from human exfoliated deciduous teeth. Proc Natl Acad Sci U S A 100:5807–5812.
42. Bishop ET, GT Bell, S Bloor, IJ Broom, NF Hendry and DN Wheatley. (1999). An in vitro model of angiogenesis: basic features. Angiogenesis 3:335–344.
43. di Summa PG, DF Kalbermatten, W Raffoul, G Terenghi and PJ Kingham. (2013). Extracellular matrix molecules enhance the neurotrophic effect of Schwann cell-like differentiated adipose-derived stem cells and increase cell survival under stress conditions. Tissue Eng Part A 19:368–379.
44. Caddick J, PJ Kingham, NJ Gardiner, M Wiberg and G Terenghi. (2006). Phenotypic and functional characteristics of mesenchymal stem cells differentiated along a Schwann cell lineage. Glia 54:840–849.
45. Kingham PJ, MK Kolar, LN Novikova, LN Novikov and M Wiberg. (2014). Stimulating the neurotrophic and angiogenic properties of human adipose-derived stem cells enhances nerve repair. Stem Cells Dev 23:741–754.
46. Bain JR, SE Mackinnon and DA Hunter. (1989). Functional evaluation of complete sciatic, peroneal, and posterior tibial nerve lesions in the rat. Plast Reconstr Surg 83:129–138.
47. Kanaya F, J Firrell, TM Tsai and WC Breidenbach. (1992). Functional results of vascularized versus nonvascularized nerve grafting. Plast Reconstr Surg 89:924–230.

48. Bertani N, P Malatesta, G Volpi, P Sonego and R Perris. (2005). Neurogenic potential of human mesenchymal stem cells revisited: analysis by immunostaining, time-lapse video and microarray. J Cell Sci 118:3925–3936.
49. Johnson PJ, MD Wood, AM Moore and SE Mackinnon. (2013). Tissue engineered constructs for peripheral nerve surgery. Eur Surg 45. DOI: 10.1007/s10353-013-0205-0.
50. Nakamura S, Y Yamada, W Katagiri, T Sugito, K Ito and M Ueda. (2009). Stem cell proliferation pathways comparison between human exfoliated deciduous teeth and dental pulp stem cells by gene expression profile from promising dental pulp. J Endod 35:1536–1542.
51. Yang J, H Wu, N Hu, X Gu and F Ding. (2009). Effects of bone marrow stromal cell-conditioned medium on primary cultures of peripheral nerve tissues and cells. Neurochem Res 34:1685–1694.
52. Hirata H, H Hibasami, T Yoshida, M Ogawa, M Matsumoto, A Morita and A Uchida. (2001). Nerve growth factor signaling of p75 induces differentiation and ceramide-mediated apoptosis in Schwann cells cultured from degenerating nerves. Glia 36:245–258.
53. Sofroniew MV, CL Howe and WC Mobley. (2001). Nerve growth factor signaling, neuroprotection, and neural repair. Annu Rev Neurosci 24:1217–1281.
54. Vogelin E, JM Baker, J Gates, V Dixit, MA Constantinescu and NF Jones. (2006). Effects of local continuous release of brain derived neurotrophic factor (BDNF) on peripheral nerve regeneration in a rat model. Exp Neurol 199:348–353.
55. Takemura Y, S Imai, H Kojima, M Katagi, I Yamakawa, T Kasahara, H Urabe, T Terashima, H Yasuda, et al. (2012). Brain-derived neurotrophic factor from bone marrow-derived cells promotes post-injury repair of peripheral nerve. PLoS One 7:e44592.
56. Woolley AG, KJ Tait, BJ Hurren, L Fisher, PW Sheard and MJ Duxson. (2008). Developmental loss of NT-3 in vivo results in reduced levels of myelin-specific proteins, a reduced extent of myelination and increased apoptosis of Schwann cells. Glia 56:306–317.
57. Quigley AF, KJ Bulluss, IL Kyratzis, K Gilmore, T Mysore, KS Schirmer, EL Kennedy, M O'Shea, YB Truong, et al. (2013). Engineering a multimodal nerve conduit for repair of injured peripheral nerve. J Neural Eng 10:016008.
58. Kang SS, MP Keasey, J Cai and T Hagg. (2012). Loss of neuron-astroglial interaction rapidly induces protective CNTF expression after stroke in mice. J Neurosci 32: 9277–9287.
59. Dinis TM, G Vidal, RR Jose, P Vigneron, D Bresson, V Fitzpatrick, F Marin, DL Kaplan and C Egles. (2014). Complementary effects of two growth factors in multifunctionalized silk nanofibers for nerve reconstruction. PLoS One 9:e109770.
60. Barras FM, P Pasche, N Bouche, P Aebischer and AD Zurn. (2002). Glial cell line-derived neurotrophic factor released by synthetic guidance channels promotes facial nerve regeneration in the rat. J Neurosci Res 70:746–755.
61. Roam JL, PK Nguyen and DL Elbert. (2014). Controlled release and gradient formation of human glial-cell derived neurotrophic factor from heparinated poly(ethylene glycol) microsphere-based scaffolds. Biomaterials 35:6473–6481.
62. Ho PR, GM Coan, ET Cheng, C Niell, DM Tarn, H Zhou, D Sierra and DJ Terris. (1998). Repair with collagen tubules linked with brain-derived neurotrophic factor and ciliary neurotrophic factor in a rat sciatic nerve injury model. Arch Otolaryngol Head Neck Surg 124:761–766.
63. Coultas L, K Chawengsaksophak and J Rossant. (2005). Endothelial cells and VEGF in vascular development. Nature 438:937–945.
64. Lee EJ, HW Park, HJ Jeon, HS Kim and MS Chang. (2013). Potentiated therapeutic angiogenesis by primed human mesenchymal stem cells in a mouse model of hindlimb ischemia. Regen Med 8:283–293.
65. Van Belle E, B Witzenbichler, D Chen, M Silver, L Chang, R Schwall and JM Isner. (1998). Potentiated angiogenic effect of scatter factor/hepatocyte growth factor via induction of vascular endothelial growth factor: the case for paracrine amplification of angiogenesis. Circulation 97:381–390.
66. Gu Y, J Zhu, C Xue, Z Li, F Ding, Y Yang and X Gu. (2014). Chitosan/silk fibroin-based, Schwann cell-derived extracellular matrix-modified scaffolds for bridging rat sciatic nerve gaps. Biomaterials 35:2253–2263.
67. Worth DC and M Parsons. (2008). Adhesion dynamics: mechanisms and measurements. Int J Biochem Cell Biol 40:2397–2409.
68. Koh HS, T Yong, CK Chan and S Ramakrishna. (2008). Enhancement of neurite outgrowth using nano-structured scaffolds coupled with laminin. Biomaterials 29:3574–3582.

Address correspondence to:
Dr. Wataru Katagiri
Department of Oral and Maxillofacial Surgery
Nagoya University Graduate School of Medicine
65 Tsuruma-cho
Showa-ku
Nagoya 466-8550
Japan

E-mail: w-kat@med.nagoya-u.ac.jp

Received for publication March 17, 2015
Accepted after revision July 6, 2015
Prepublished on Liebert Instant Online July 8, 2015